Energy dependence of the optical-model potential for fast-neutron scattering from bismuth

R. D. Lawson, P. T. Guenther, and A. B. Smith
Argonne National Laboratory, Argonne, Illinois 60439
(Received 22 May 1987)

Neutron differential-elastic-scattering cross sections of bismuth were measured at ≈0.5 MeV intervals from ≈4.5 to 10.0 MeV. At each incident energy 40 or more differential values were obtained between ≈18° and 160°. These data were combined with lower-energy results previously reported from this laboratory, and others available in the literature, to provide a detailed data base extending from ≈1.5 to 10.0 MeV. This data base was interpreted in terms of the conventional optical-statistical model and also using a model which included the surface-peaked real potential predicted by the dispersion relation. Particular attention was given to the energy dependence of the volume-integral-per-nucleon of the real potential, J_v, to see if there was evidence of the Fermi surface anomaly. In the range 3.0–10.0 MeV, the present study indicates that dJ_v/dE is essentially constant, with a relatively large negative value of −6.0 to −9.0 fm^3, depending on the model used in the analysis. Below 3.0 MeV, there is some evidence for a decrease in the magnitude of dJ_v/dE. However, the effect is very small, and it is only when this trend is combined with considerations of the J_v values needed to give correct bound-state energies that evidence for the Fermi surface anomaly emerges. J_v and the geometry of the optical potentials found for ^{209}Bi become equal to those explaining the higher-energy ^{208}Pb data at about 10.0 MeV. Since dJ_v/dE for the latter is smaller in magnitude than that for ^{209}Bi, a change in dJ_v/dE is clearly indicated near 10.0 MeV.

I. INTRODUCTION

It has been known for many years that the observed level spacings and binding energies of the single-particle and single-hole states in ^{208}Pb can be predicted by the use of a static Woods-Saxon potential.[1] This means that the effective mass of a valence nucleon is nearly equal to its free mass, and this in turn implies that the derivative of the potential with respect to energy, dV/dE, is ≈0 near the Fermi surface,[2] an effect known as the Fermi surface anomaly. Mahaux and Ngô[3] have made detailed studies of the polarization and correlation contributions to the optical-model potential for ^{208}Pb. They predict that below about 6.0 MeV the real potential has a highly nonlinear energy dependence and that dV/dE becomes zero near $E=4.0$ MeV. Charged-particle scattering sheds little light on this phenomena since the energies of interest are at or below the Coulomb barrier. However, an analysis of the low-energy neutron elastic-scattering angular distributions, using the spherical optical-statistical model, should show this behavior. Because ^{208}Pb is a doubly-closed-shell nucleus, fluctuations in the compound-nucleus cross section are large and can strongly affect the analysis of low-energy neutron scattering data. On the other hand, the neighboring element, ^{209}Bi, is monoisotopic, and has a high density of states near the neutron binding energy. Therefore, it offers the opportunity for study of energy-averaged neutron cross sections, consistent with the concept of the optical model, down to fairly low energies without undue perturbations from fluctuation effects.

There have been several comprehensive studies of elastic-neutron scattering from ^{209}Bi in the incident energy range from several hundred keV to approximately 4.0 MeV.[4–6] However, except for the 7.0 MeV data of Zafiratos *et al.*[7] and the ≈6.0, 7.0, and 8.0 MeV distributions of Holmqvist and Wiedling,[8] there was little information available above 4.0 MeV until the recent work of Annand *et al.*,[9] who reported detailed measurements in the 4.0–7.0 MeV range. In this paper we report twelve new neutron elastic-scattering angular distributions, distributed in energy from 4.5 to 10.0 MeV at intervals of approximately 0.5 MeV. These new data were combined with the lower-energy results of Refs. 5 and 6 to provide a detailed data base, extending over the energy range 1.5–10.0 MeV, for neutron scattering from ^{209}Bi. This data base was then analyzed using spherical optical-statistical-model theory to determine the best parametrization of the model, and to examine the energy dependence of J_v, the volume-integral-per-nucleon of the real potential, over the energy range 1.5–10.0 MeV.

In Sec. II we briefly discuss the experimental methods used to obtain the data, and the experimental results are presented in Sec. III. Section IV contains a description of the two variants of the optical model used in the interpretation of the data: first, the conventional optical-statistical model in which the real potential was taken to have the Woods-Saxon form; and second, the model in which a surface-peaked component predicted by the dispersion relationship[2] is added to this well. In Sec. V the properties of the ^{209}Bi optical-model potential are discussed and evidence for the Fermi surface anomaly is presented. Also, in this section it is shown that a combined interpretation of the ^{208}Pb and ^{209}Bi data leads to

the conclusion that dJ_v/dE changes its magnitude near $E=10.0$ MeV. Finally, in Sec. VI the findings of this work are summarized.

II. EXPERIMENTAL METHODS

The time-of-flight methods used in the present measurements have been extensively employed at the Argonne Tandem Dynamitron. Since they have been described in detail on a number of occasions,[10–12] only a brief outline is given here.

The measurement samples were solid cylinders 2 cm in diameter by 2 cm long. The neutrons were incident on their lateral surfaces. The bismuth sample was cast of chemically pure metal and machined to size. The polyethylene reference sample was machined from commercially available material. Sample densities were determined to better than 0.01% using conventional measurement techniques.

The ^{2}H(d,n)^{3}He reaction[13] was used as the neutron source throughout the measurements. The mean neutron energies were determined to $\approx$25 keV by control of the incident-deuteron beam. The deuteron-gas target was contained in a cell $\approx$3.5 cm long, at pressures resulting in neutron energy spreads at the sample of $\approx$100–200 keV, decreasing with increasing energy. The deuteron beam was pulsed at a 2 MHz repetition rate, with a burst duration of $\approx$1 nsec. The scattering samples were placed 15–18 cm from the source at a zero-degree reaction angle.

The measurements were made using the Argonne 10-channel time-of-flight apparatus.[12] The time spectra of neutrons scattered over flight paths of $\approx$503 cm were concurrently measured at ten scattering angles. The angular setting of the entire apparatus was varied several times to obtain differential cross sections at 40 or more angles at each incident energy. Two additional time channels provided redundant monitoring of the neutron-source intensity. Relative detector sensitivities were determined using the well-known spectrum of neutrons emitted from a spontaneously fissioning ^{252}Cf source, as described in Ref. 14. The absolute sensitivity of the detector system was determined relative to the H(n,n) scattering standard[15] using polyethylene, CH_2, as the hydrogeneous scattering sample. The observed scattering distribution from bismuth and from hydrogen were corrected for multiple-event, angular-resolution, and incident-beam-attenuation effects using analytical and Monte Carlo methods.[16]

III. EXPERIMENTAL RESULTS

Differential neutron-elastic-scattering distributions were measured for twelve incident-neutron energies between 4.5 and 10.0 MeV, at approximately 0.5-MeV intervals. Each distribution consisted of at least 40 differential cross sections ($\approx$100 at some energies) distributed over the angular range $\approx$18°–160°. The scattered-neutron energy resolution was sufficient to separate the elastically scattered neutron group from all known inelastically scattered components. Some of the latter data were reduced to cross sections, but since they are not germane to the present considerations they will be reported elsewhere.[17] Throughout the measurements, differential elastic-scattering cross sections of carbon were also concurrently determined at each energy in order to verify the fidelity of the measurement system relative to the well-known carbon values.[15]

At most scattering angles the statistical uncertainties (foreground and background) were relatively small ($\lesssim$1%), but they could be considerably larger at the deep minima of the distributions. The neutron detector calibrations were believed known to $\lesssim$3%. This conclusion was supported by the consistency of results obtained many months apart with essentially independent instrument calibrations. The relative neutron-scattering angles were optically established to $\lesssim$0.1°. The absolute calibration of this angular system was determined to $\pm\lesssim$0.25° at each measurement period by observing forward-angle neutron scattering both left and right of the apparent center line. For heavy nuclei the elastic-scattering cross section varies rapidly with angle. Thus even these small angular uncertainties can make a major contribution to the overall experimental uncertainty at some angles. The correction procedures introduced additional uncertainties, generally $\lesssim$1%, but larger near the minima of the distributions. There were systematic uncertainties associated with sample masses and the H(n,n) reference cross sections; both were relatively small ($\lesssim$1%). These various sources of experimental error were combined in quadrature to obtain the total experimental uncertainty. In addition, a minimum uncertainty of 2 mb/sr was assumed as representative of unknown error sources and general detection sensitivity. The latter contributions can be significant at the minima of the distributions. Finally, it should be pointed out that the measurement method involved the use of ten essentially independent detection systems, resulting in a considerable degree of redundancy that made possible the verification of a number of the above uncertainty estimates.

The experimental results, with their uncertainties, are shown in Fig. 1. Prior directly comparable results are remarkably sparse and are largely summarized in Fig. 2. The results of Ref. 8 are reasonably consistent with the present values at $\approx$7 and 8 MeV, but are less so at $\approx$6 MeV. The $\approx$6 MeV results of Ref. 18 differ at some angles from the present values, and the same is true for the $\approx$7-MeV results of Ref. 19. However, the 7-MeV results of Ref. 7 are in excellent agreement with those of the present work. More recently, Annand *et al.*[9] have reported results in the 4- to 7-MeV range and, judging from their figures, their values seem to be consistent with those of the present work. The present experimental results nicely extrapolate to the lower-energy ($\lesssim$4.0 MeV) values previously reported from this laboratory[5] and to those of Olsson *et al.*,[6] as illustrated in Fig. 1.

IV. OPTICAL-MODEL INTERPRETATIONS

The optical-model interpretations were based upon three sets of differential-elastic-scattering data: (i) the

present results extending from 4.5 to 10.0 MeV, (ii) the 1.5–4.0 MeV results reported earlier from this laboratory,[5] and (iii) the ≈1.5–4.0 MeV results reported by Olsson *et al.*[6] Specification of the experimental uncertainties is essential for quantitative interpretation, and thus the present work gave considerable attention to their definition, as described in Sec. III. The earlier work of Ref. 5 was carried out with an applied objective and does not have the accuracy of the present results, but it is in good agreement with the values of Ref. 6. Furthermore, the experimental uncertainties are reasonably well defined. The uncertainties associated with the work of Ref. 6 are not as clearly specified, either in the journal paper or in the underlying laboratory report. Therefore, a simple assumption of equal percentage uncertainties for all datum values was made. An additional data set extending from 0.3 to 1.5 MeV has been reported by some of the present authors.[4] It was not used in these analyses as it involves relatively low energies where the assumptions underlying the use of the optical model may not be valid due to evident fluctuations. There are a few other differential-elastic-scattering distributions in the 1.5–10.0 MeV energy range reported in the literature and available from the files of the National Nuclear Data Center, Brookhaven National Laboratory. Some of this additional information was not available in numerical form and thus could not be used. In the cases where numerical results were available they tended to support the above three primary data sets, as illustrated in Fig. 2.

A. Conventional optical model potential

Initially, a conventional spherical optical-statistical model was assumed, consisting of a Woods-Saxon real potential, a Woods-Saxon-derivative imaginary well, and a Thomas spin-orbit interaction.[20] Below ≈6.5 MeV, compound-nucleus affects were a concern and were calculated using the Hauser-Feshbach formula,[21] as modified for width fluctuation and correlation corrections by Moldauer.[22] Discrete states were included in the calculations to an excitation energy of ≈3.2 MeV, using the spin and parity assignments of Lederer and Shirley.[23] Above this energy, the target level density was computed from the formula

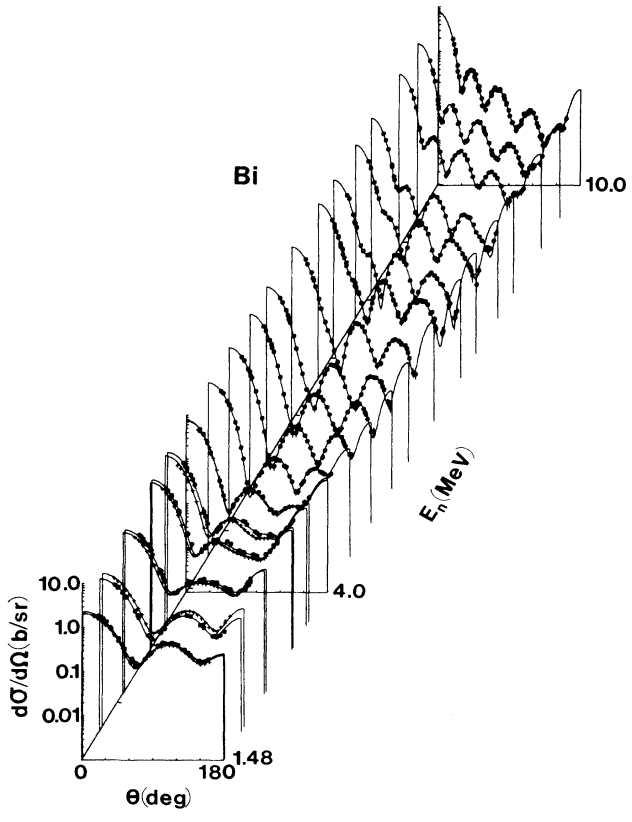

FIG. 1. The present experimental results for $E \geq 4.5$ MeV together with the lower-energy ($E \leq 4.0$ MeV) values previously reported from this laboratory (Ref. 5), ○, and as given in Ref. 6, +. For clarity, values from Refs. 5 and 6 are shown only at ≈0.5 MeV intervals. Curves are eyeguides. Scattering angles and neutron energies are in the laboratory system.

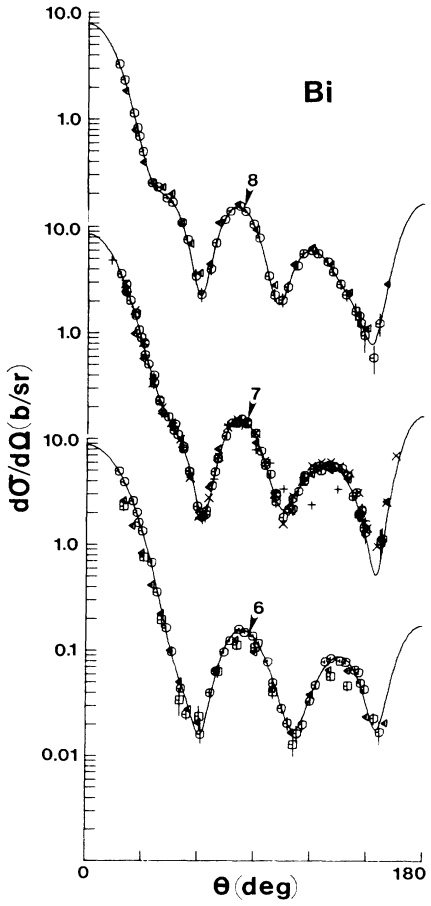

FIG. 2. Comparison of the present experimental results (○) with those reported in the literature (×, Ref. 7; ◁, Ref. 8; □, Ref. 18; +, Ref. 19). Approximate neutron energies in MeV are noted numerically. Curves are eyeguides. Scattering angles and neutron energies are given in the laboratory system.

$$\rho(E,J)=\frac{(2J+1)}{2\sigma^2 T}\exp[(E-E_0)/T]\exp[-(J+\tfrac{1}{2})^2/2\sigma^2] , \tag{1}$$

where J is the angular momentum of the continuum target level and E_0, T, and σ are parameters. No values for these parameters are given by Gilbert and Cameron[24] for ^{209}Bi. However, all the bismuth isotopes they considered have about the same value for the spin-cutoff parameter, $\sigma \approx 4.4$, and that value was used in the present calculations. In the incident-neutron energy range 3.2–6.5 MeV, compound-elastic scattering contributes very significantly to the magnitude of the differential cross section at the back-angle minima. Consequently, with σ fixed, E_0 and T were adjusted so as to best reproduce these cross-section minima. The resulting level-density parameters were

$$\begin{aligned} E_0 &= 0.1 \text{ MeV} , \\ T &= 1.15 \text{ MeV} , \\ \sigma &= 4.4 . \end{aligned} \tag{2}$$

The derivation of the optical-model potential from the measured values was based upon χ^2 fitting procedures, minimizing the quantity

$$\chi^2=\Sigma_i \left[\frac{\sigma_{\text{exp}}(\theta_i)-\sigma_{\text{cal}}(\theta_i)}{\delta\sigma_{\text{exp}}(\theta_i)} \right]^2 , \tag{3}$$

where $\delta\sigma_{\text{exp}}(\theta_i)$ is the experimental uncertainty associated with the elastic-scattering cross section, $\sigma_{\text{exp}}(\theta_i)$, of the data base and $\sigma_{\text{cal}}(\theta_i)$ is the calculated value. The fitting procedures started with a subjective examination of the spin-orbit potential, using distributions in the 9- to 10-MeV range where the observables are more sensitive to this potential. Six-parameter fits were made (concurrently varying real and imaginary strengths, radii, and diffusenesses), using a mesh of spin-orbit-potential strengths and geometries. From these considerations, the parameters characterizing the spin-orbit interaction were deduced to be

$$\begin{aligned} V_{\text{so}} &= 5.22 \text{ MeV} , \\ r_{\text{so}} &= 1.005 \text{ fm} , \\ a_{\text{so}} &= 0.65 \text{ fm} . \end{aligned} \tag{4}$$

These values were held constant throughout the remainder of the fitting. In all cases the nuclear radii of the potentials are given by $R_i = r_i A^{1/3}$. The possibility of a contribution from volume absorption at these higher energies was also examined, but no evidence for this interaction was found.

With the fixed spin-orbit strength, each of the distributions of the entire data base was fitted using six adjustable parameters, with particular attention given to the values of the new 4.5–10.0 MeV measurements. The results of this fitting indicated a relatively stable imaginary radius, so this parameter was fixed to the average value of $r_w = 1.3102$ fm for subsequent five-parameter fits to the entire data base. The latter indicated an energy-dependent real radius given by $r_v = [1.36 - 0.0175 \times E(\text{MeV})]$ fm. The fitting procedure was then repeated using four parameters, and the resulting imaginary diffuseness was selected as the most stable of the remaining geometric parameters. It displayed a strong energy dependence given by $a_w = [0.05 + 0.055 \times E(\text{MeV})]$ fm. Proceeding in a similar manner through a three-parameter fitting process, the real diffuseness $a_v = [0.54 + 0.02 \times E(\text{MeV})]$ fm was obtained, where the energy dependence was slight, if present at all. Thus, the final geometric parameters were taken to be

$$\begin{aligned} r_v &= (1.36 - 0.0175 \times E) \text{ fm} , \\ r_w &= 1.3102 \text{ fm} , \\ a_v &= (0.54 + 0.02 \times E) \text{ fm} , \\ a_w &= (0.05 + 0.055 \times E) \text{ fm} , \end{aligned} \tag{5}$$

where E is the incident energy in MeV. Using this geometry, two-parameter fits were carried out in which the real and imaginary potential strengths were varied. A very good description of the entire data base was then obtained, as illustrated in Fig. 3. Moreover, although not shown, these parameters can be extrapolated to give a reasonable description of the very low energy (0.3–1.5 MeV) data of Ref. 4. The resulting real and imaginary potential strengths, expressed as volume-integrals-per-nucleon [$J_i = (4\pi/A) \int V_i(r) r^2 dr$], are shown in Fig. 4. If one considers only the new 4.5–10.0 MeV data, the J_i values have a linear dependence on energy, E (in MeV), given by

$$\begin{aligned} J_v &= [(459.78 \pm 2.41) - (9.58 \pm 0.32) \times E] \text{ MeV fm}^3 , \\ J_w &= [(33.87 \pm 2.70) - (1.05 \pm 0.37) \times E] \text{ MeV fm}^3 , \end{aligned} \tag{6}$$

where the errors in the coefficients are almost exactly anticorrelated. In deducing these uncertainties a constant percentage error for each of the twelve values of J_v (J_w) was assumed, and this percentage adjusted to give χ^2 per degree of freedom the value unity in each case. The values of Eqs. (6) are illustrated by the solid lines shown in Fig. 4. It appears that below ≈ 3.0 MeV, Eq. (6) tends to overestimate the value of J_v obtained from the optical-model fits. This point is discussed further in the next section.

B. Surface-peaked real potential

The real optical-model potential is related to the imaginary interaction through the dispersion relation[2]

$$V(r,E)=V_{\text{WS}}(r,E)+\frac{P}{\pi}\int_{-\infty}^{+\infty}\frac{W(r,E')dE'}{(E-E')} , \tag{7}$$

where P stands for the principal-value integral, and $V_{\text{WS}}(r,E)$ is the Hartree-Fock potential which is taken to have the Woods-Saxon shape. This relation results in a surface-peaked addition to the real potential with a magnitude given by the integral of Eq. (7). Because the geometrical factors in $W(r,E')$ are energy dependent, it

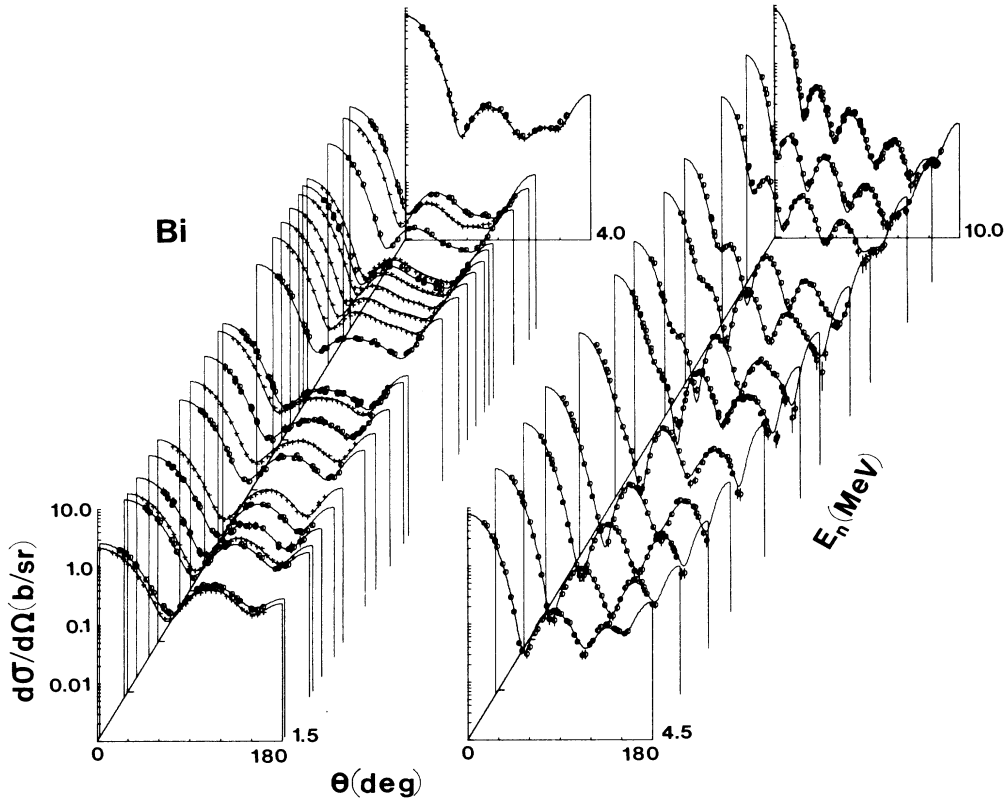

FIG. 3. Comparison of measured values (○ indicating the present work, an ≈200 keV average of that of Ref. 5, and + that of Ref. 6) and the calculated results (curves) obtained using the conventional optical model, Sec. IV A of the text.

is more convenient to find the magnitude of this added potential from considerations involving $J_w(E')$. The quantity

$$\lambda(E)=\left[\frac{P}{\pi}\int_{-\infty}^{+\infty}\frac{J_w(E')dE'}{E-E'}\right]\Big/J_w(E)\ , \tag{8}$$

is the factor by which $W(r,E)$ must be multiplied to give the surfaced-peaked contribution to the real potential.[25] In evaluating the principal-value integral it has been assumed that J_w is symmetric about the Fermi energy (taken to be $E_F=-5.65$ MeV) and, in the energy range $2E_F\leq E'\leq 0$, is proportional to $(E-E_F)^2$.[26] In the range $0\leq E'\leq 10.09$ MeV,

$$J_w=30.93+1.37\times E'\ , \tag{9}$$

which is the best linear fit to all of the data points shown in Fig. 4. For the $10.09\leq E'\leq 49.34$ MeV range, the surfaced-peaked imaginary potential of Walter and Guss[27] was used. The upper end of the energy range was dictated by the fact that the Walter-Guss potential goes to zero at that value of E'. The lower end, 10.09 MeV, was chosen to make J_w continuous, and, in addition, the function was made continuous at $E'=0$. The resulting values of $\lambda(E)$ are shown in Fig. 5(a).

The data were refitted including the surface-peaked real potential. The level-density parameters and the spin-orbit interaction were held fixed with the values of Eqs. (2) and (4), respectively. In a manner analogous to that described in Sec. IV A, the geometric parameters of the real and imaginary potentials were deduced to be

$$\begin{aligned} r_v&=(1.28-0.007\times E)\text{ fm}\ ,\\ r_w&=1.3022\text{ fm}\ ,\\ a_v&=0.68\text{ fm}\ ,\\ a_w&=(0.119+0.043\times E)\text{ fm}\ , \end{aligned} \tag{10}$$

where E is the energy in MeV. The value of r_w is essentially identical to that obtained with the conventional model. On the other hand, since a surface-peaked potential whose strength, as shown in Fig. 5(a), decreases with increasing energy has been added, a slower energy variation of r_v than for the conventional model should be anticipated. Moreover, r_v in this case should be smaller at low energies than the value given by the conventional model, but the two quantities should approach each other in the 9.0 MeV region where $\lambda(E)$ goes to zero. Comparison of Eqs. (5) and (10) shows these expectations are borne out. The imaginary diffuseness again has a rapid energy variation, whereas a_v is energy independent in this case. Using these geometric factors, two-parameter fits were made and again a good descrip-

tion of the data was obtained, as illustrated in Fig. 6. Qualitatively, the fit is similar to that obtained with the conventional model, Fig. 3, but close inspection of Fig. 6 indicates some improvement in the description, and this is supported by generally smaller χ^2 values resulting from this fitting.

The values obtained for the volume-integrals-per-nucleon of the imaginary interaction and the real Woods-Saxon potential are shown in Figs. 5(b) and 5(c), respectively. If one restricts oneself to the new 4.5–10.0 MeV data, a best fit to these values gives

$$J_{\rm WS}=[(422.41\pm2.46)-(4.83\pm0.33)\times E]\ \text{MeV fm}^3\ ,$$
$$J_w=[(31.03\pm2.48)+(1.41\pm0.34)\times E]\ \text{MeV fm}^3\ , \tag{11}$$

where again E is the energy in MeV, and the uncertainties in the coefficients were determined in the manner described in the discussion of Eq. (6). Considering the uncertainties in the coefficients, the form of J_w is quite similar to that obtained with the conventional model, Eq. (6). The parameters describing the variation of $J_{\rm WS}$ with energy cannot be compared directly with the values of J_v given in Eq. (6) because $J_{\rm WS}$ is the volume-integral-per-nucleon of only the Woods-Saxon part of the real potential. The quantity comparable to J_v is the sum of $J_{\rm WS}$ and $\lambda(E)J_w$, and this will be discussed later.

Because the geometry and strength of the imaginary potential are changed slightly from the values of the conventional model, the magnitude of the principal-value integral, Eq. (8), also changes. Thus, in order to do the calculations in a self-consistent manner, $\lambda(E)$ must be recalculated using the new form of J_w, and the fitting redone with this new magnitude of the added surface real potential. New values of $\lambda(E)$ were calculated and fits performed at several energies. The results obtained were so close to the values given in the initial iteration that the more comprehensive self-consistent calculations were deemed unnecessary.

V. DISCUSSION

Since the level-density parameters largely determine the levels sharing in the reaction cross section, the predicted inelastic excitation of the first two levels at 897 keV ($\frac{7}{2}^-$) and 1.608 MeV ($\frac{13}{2}^+$) should be sensitive to these quantities. With the values of Eq. (2), the predicted cross sections for the excitation of these two states at, for example, 5.0 MeV incident energy are 110 and 77 mb, respectively, using the conventional optical model.

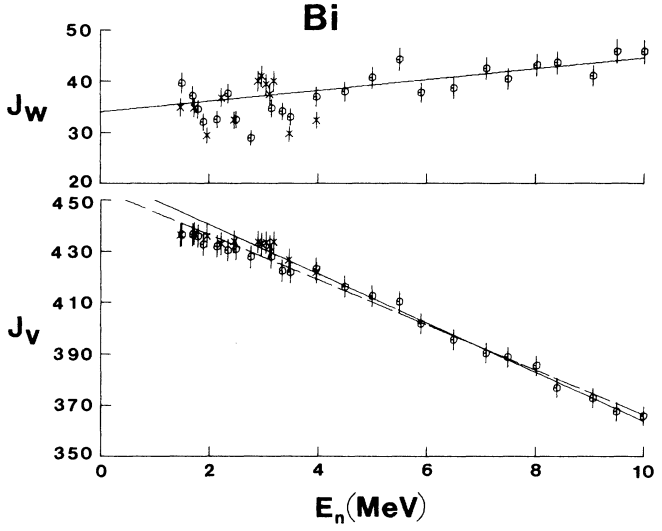

FIG. 4. The volume-integral-per-nucleon of the imaginary interaction, J_w, and the real potential, J_v (in MeV fm^3), resulting from the conventional optical-model fit to the data, as described in Sec. IV A. The solid lines represent the fit to these volume integrals, Eq. (6), when only the 4.5–10.0 MeV data are used. The broken line in the J_v figure shows the fit when all J_v values are considered, Eq. (12). The ○ symbols indicate values derived from the present measurements and those of Ref. 5 and × those derived from the experimental values of Ref. 6. Here, and throughout the figures of this paper, the illustrated uncertainties associated with J_v (and $J_{\rm WS}$) and J_w are 1% and 5%, respectively. They are subjective estimates, supported by considerations of reproducibility.

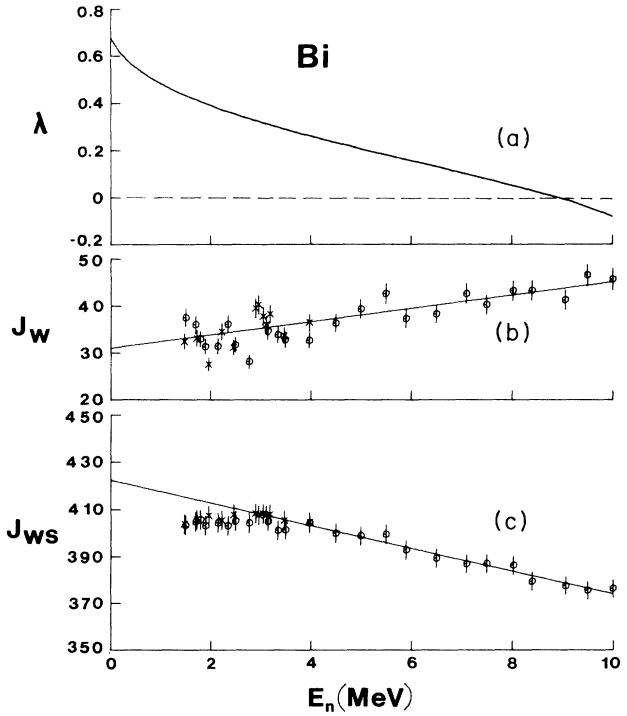

FIG. 5. Part (a), the quantity $\lambda(E)$, Eq. (8), which when multiplied by $W(r,E)$ gives the value of the surface peaked real potential, is shown as a function of laboratory energy. Parts (b) and (c) show the energy variation of the volume-integral-per-nucleon (in MeV fm^3) of the surface-peaked imaginary interaction, J_w, and the real Woods-Saxon potential, $J_{\rm WS}$, respectively, for the model described in Sec. IV B of the text. The solid curves indicate the best fit to the 4.5–10.0 MeV data, Eq. (11). The data symbols have the same connotation as in Fig. 4.

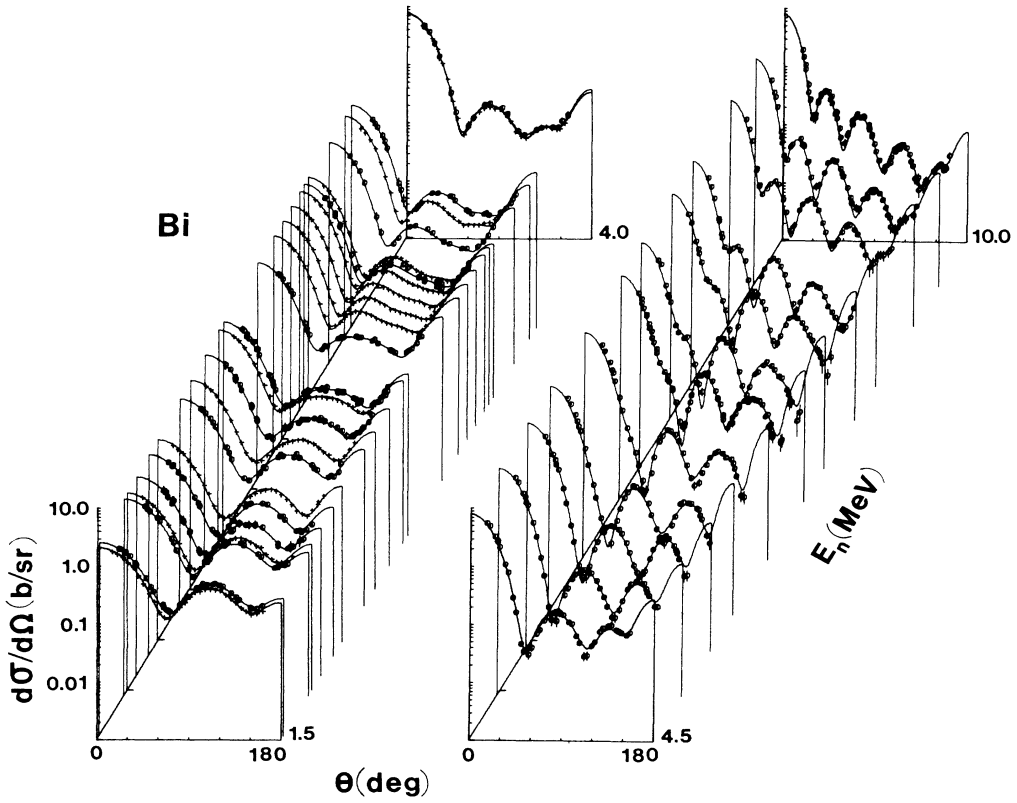

FIG. 6. Comparison of measured values (○ indicating the present work and that of Ref. 5, and + that of Ref. 6) and the results calculated with the surface-peaked potential described in Sec. IV B of the text (curves).

The values changed by $\lesssim 1.5\%$ if the surface-peaked model is used. These predictions are in good agreement with the measured values reported by Annand *et al.*[9] If T changes by $\pm 10\%$ the predicted inelastic cross sections are changed by approximately $\pm 25\%$. On the other hand, the results are less sensitive to changes in E_0, where a ± 0.1 MeV change alters the predicted inelastic cross sections by approximately $\pm 5\%$. Thus the combination of fitting the back-angle minima of the elastic-scattering cross section and the correct prediction of the inelastic excitation of the $\frac{7}{2}^-$ and $\frac{13}{2}^+$ levels puts stringent restrictions on the nuclear temperature, T.

The spin-orbit parameters were held fixed for the present interpretations. Since the predicted neutron polarization depends on the spin-orbit strength, it is of interest to see that Eq. (4) gives the correct magnitude of this quantity. The polarization was calculated at 7.75 MeV using both the conventional [Eqs. (4)–(6)] and surface-peaked [Eqs. (4), (8), (10), and (11)] models and compared with experimental results of Bulski *et al.*[28] Either model gave a satisfactory description of the experimental values as illustrated in Fig. 7.

In both models the geometries of the real and imaginary potentials are energy dependent, see Eqs. (5) and (10). For the real potential, r_v decreases with increasing energy and this energy dependence is particularly strong for the conventional model. For both models, r_v is relatively large (≈ 1.3 fm) at low energies compared to values resulting from the interpretation of higher-energy data. This dichotomy between r_v values deduced from low- and high-energy studies is frequently evident in the literature. On the other hand, the diffuseness of the real

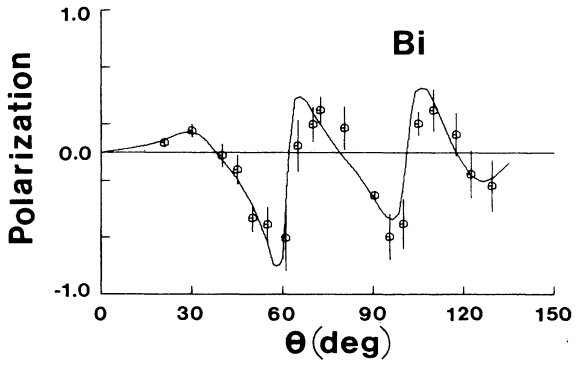

FIG. 7. Comparison of measured (Ref. 28) (symbols) and calculated (curve) polarizations resulting from the elastic scattering of 7.75 MeV neutrons from ^{209}Bi. The calculations used the conventional potential of Sec. IV A. Very similar calculated results are obtained using the surface-peaked potential of Sec. IV B. The results are shown in the center-of-mass system.

Woods-Saxon potential, a_v, is energy independent for the surface-peaked model and exhibits only a small (if significant) increase with energy for the conventional model. The imaginary potentials in the two cases are quite similar, as one would expect since the surface-peaked term affects only the real interaction. The imaginary radii, r_w, are almost identical and energy independent. However, the imaginary diffuseness, a_w, rapidly increases with energy, going from a near delta-function value ($a_w \rightarrow 0$) at zero energy to $a_w = 0.6$ and 0.549 fm at 10.0 Mev for the conventional and surface-peaked models, respectively. Thus, by 8.0–10.0 MeV the imaginary diffusenesses have values similar to those usually given by global analyses,[29] but at low energies the diffusenesses are quite small, as reported in earlier studies of this nucleus.[5,9]

As can be seen from Eq. (6), the volume-integral-per-nucleon of the real potential decreases with increasing energy for the conventional model. The decrease for ^{209}Bi is much more rapid than it it is in the $A = 90$ region,[25–30] and as given in global representations.[29] The Woods-Saxon portion of the real surface-peaked potential, Eq. (11), also decreases with energy, with a slope approximately half that deduced from the conventional model. This is to be compared to the energy-independent value found for this quantity is an analysis of neutron elastic scattering from yttrium.[25] For both models, the volume-integral-per-nucleon of the imaginary potential is small, a characteristic of nuclei near closed shells,[31] and exhibits a modest increase in value with energy.

Each of the models presented in Sec. IV will now be discussed in detail in order to examine to what extent they throw light on the Fermi surface anomaly.

A. Conventional optical model potential

As can be seen from Fig. 4, the 3.0–10.0 MeV values of J_v, extracted from the fit to the ^{209}Bi data, lie on a straight line with a slope considerably larger than obtained by Rapaport[29] in his global analysis of 7.0–30.0 MeV neutron data. Below 3.0 MeV the J_v values fall consistently below the solid curve, Eq. (6), which illustrates the fit to the 4.5–10.0 MeV data. Furthermore, even with a best fit to all the ^{209}Bi J_v values, namely

$$J_v = [(454.18 \pm 1.07) - (8.80 \pm 0.21) \times E] \text{ MeV fm}^3 , \tag{12}$$

the low-energy values still fall below the curve. This deviation from linearity is small ($\lesssim 2\%$ at 1.5 MeV), and occurs in an energy region where compound-elastic scattering significantly influences the choice of model parameters. The present interpretation uses the Hauser-Feshbach theory,[21] with the most recent Moldauer formulation of width-fluctuation and correlation corrections.[22] Detailed numerical studies by Moldauer[22] showed that this correction procedure is equivalent to that of Tepel *et al.*,[32] and Annand *et al.*[9] show that both give results in this mass-energy region very similar to those obtained with the correction procedures of Hofmann *et al.*[33] However, there is a haunting concern for the validity of the theoretical description at the lower energies. It would be interesting to reinterpret the above data using alternate formulations of statistical-reaction theory (i.e., as described by Zirnbauer[34]), but the means to investigate such new concepts was not available to the authors. The ^{209}Bi total cross sections are known to fluctuate by considerable amounts to well over 2.0 MeV,[35] and it is reasonable to expect an enhancement of these fluctuations in the elastic channel. Their magnitude and spacing is such that it is not clear that the observed lower-energy differential-elastic-scattering cross sections, even with the relatively coarse experimental resolutions involved, truly represent an energy-averaged behavior consistent with the optical-model concept. This concern is somewhat mitigated by the good agreement between the 1.5–4.0 MeV results of Ref. 5, which were generally averaged over 200 keV intervals, and the "monoenergetic" distributions of Ref. 6 in the same energy range. However, a close inspection of Fig. 4, while showing no visible sign of fluctuations in the J_v values, suggests that there are fluctuations in the J_w values at lower energies. Moreover, the variations of J_w with energy following from the independent experimental values of Refs. 5 and 6 tend to be very similar.

Although the ^{209}Bi data seem to result in a small decrease in the absolute value of dJ_v/dE as one goes below 3.0 MeV, the above arguments show how difficult it is to make a definitive statement about this point from a study of low-energy neutron-scattering data alone. On the other hand, the bound-state data do show that dJ_v/dE becomes small, and perhaps even changes sign, for $E < 0$. If one uses the spin-orbit strength of Eq. (4), the $E = 0$ geometry of Eq. (5) for the Woods-Saxon potential, and adjusts the well depth to reproduce the binding energies[36,37] of the seven known single-particle and six hole states, one finds that the average values of J_v for these states are 438.7 and 433.8 MeV fm^3, respectively. Thus the most one can say from the neutron scattering viewpoint is that the tendency for the J_v values to level off below 3.0 MeV is consistent with the results needed to give the correct bound-state energies.

In a similar study Annand *et al.*[9] combined data for ^{208}Pb and ^{209}Bi to examine the behavior of J_v over a wide energy range. From a detailed fit to their 6.0, 6.5, and 7.0 MeV data, and to the 20.0, 22.0, and 24.0 MeV ^{208}Pb results of Finlay *et al.*,[38] they concluded that the geometrical parameters of the real and imaginary wells in the 0–24.0 MeV incident-energy range should be

$$\begin{aligned} r_v &= (1.302 - 0.0055 \times E) \text{ fm} , \\ a_v &= 0.7 \text{ fm} , \\ r_w &= (1.363 - 0.0042 \times E) \text{ fm} , \\ a_w &= (0.162 + 0.0189 \times E) \text{ fm} , \end{aligned} \tag{13}$$

where E is the neutron energy in MeV. With this geometry and the spin-orbit potential fixed at $V_{so} = 6.2$ MeV, $r_{so} = 1.01$ fm, and $a_{so} = 0.75$ fm, two-parameter fits, varying V_0 and W_0, were made to the ^{208}Pb and

^{209}Bi data. For energies greater than 3.0 MeV, they found that J_v decreased with energy with $dJ_v/dE = -4.9$ MeV fm^3. However, below 3.0 MeV, their analysis of the data of Ref. 6 indicated that dJ_v/dE changed sign (i.e., at 2.961, 2.451, 1.962, and 1.475 MeV the respective J_v values were 420.8, 419.4, 417.1, and 415.4 MeV fm^3). On the other hand, our analysis of the same data ($\times$'s of Fig. 4) showed that dJ_v/dE is still negative at low energies, but somewhat less so than given by Eq. (6). Because of its implication with respect to the Fermi surface anomaly, we examined this point carefully and found that when our potential geometry, Eq. (5), was used, instead of that of Eq. (13), a much better fit to the low-energy data of Ref. 6 was obtained. Quantitatively, if $\delta\sigma_{\rm exp}(\theta_i)$ of Eq. (3) is taken to be an angle-independent fraction of $\sigma_{\rm exp}(\theta_i)$, the value of χ^2 per degree of freedom with the geometry of Eq. (5) is always at least a factor of 2 smaller than that obtained with the geometry of Eq. (13), and this factor increases with decreasing energy, reaching a value of 7.7 at the lowest energy. Thus the behavior of J_v at the low energies is critically affected by the geometry used in the analysis of the data. Furthermore, if the spin-orbit interaction of Ref. 9, together with the $E=0$ geometry given by Eq. (13), is used to deduce the values of J_v needed to give the correct particle- and hole-state binding energies, one finds that the average value for the particle states is $J_v=432.4$ MeV fm^3 and that for the hole states 426.8 MeV fm^3. In other words, dJ_v/dE must once again change sign in the region $E\approx -3.0$ to $+1.5$ MeV in order to accommodate the bound-state data. Such an extra "flip" is not theoretically expected. Alternatively, to avoid this second change of sign, the Woods-Saxon well radius for bound states must be smaller than the $E=0$ limit of Eq. (13), and such an affect has recently been suggested by Mahaux and Sartor.[39]

In order to check the extrapolation of our model to very low energies, Eqs. (5), (9), and (12) were used to obtain the parameters for calculating the S-wave strength function. The predicted value of S_0 is 1.386×10^{-4} compared to the experimentally deduced value[40] of $(0.65\pm0.15)\times10^{-4}$. Since[41]

$$S_0 \approx \int W(r)\,|\,u(r)\,|^2 dr\ , \tag{14}$$

where $u(r)$ is the nucleon wave function in the complex well and $W(r)$ is the imaginary interaction, it is clear that a smaller value of S_0 can be obtained if either W_0, the strength of the potential, or a_w, the imaginary diffuseness is changed. Equations (5) and (9) lead to $W_0=42.54$ MeV and $a_w=0.05$ fm at $E=0$. If a_w is halved, the predicted S_0 is 0.736×10^{-4}. Alternatively, halved W_0 leads to essentially the same result. Thus, to obtain a good description of the experimentally-deduced S-wave strength function, the zero-energy intercept of J_w must be reduced by about a factor of 2. An inspection of Fig. 4 shows that, below 3.0 MeV, the values of J_w extracted from a fit to the data of either Ref. 5 or 6 seem to 'oscillate" about the linear curves given by Eq. (6) and this oscillation will probably become even more pronounced as one goes toward zero energy (i.e., fluctuations will become more important). Thus a zero-energy value of J_w different from the linear extrapolation is not surprising.

Next, consider the extrapolation of Eqs. (4), (5), (9), and (12) to the calculation of total cross sections outside the 1.5–10.0 MeV energy range. In the few-hundred-keV region the model gives as good a prediction of the highly fluctuating total cross section as one can reasonably expect. This is illustrated by the $\times$'s in Fig. 8. However, above $\approx$10.0 MeV the rapid energy variation of the geometric parameters, Eq. (5), quickly leads to difficulty. On the other hand, since $[(N-Z)/A]$ is almost the same for ^{208}Pb and ^{209}Bi, it is reasonable to expect the real potential for these two nuclei to be quite similar. (If one uses Rapaport's global parameters[29] the two well depths should only differ by 132 keV.) Furthermore, although the imaginary potentials in the two cases may be quite different at low energies, above 10.0 MeV this difference should largely disappear. Thus, the analyses of the ^{208}Pb data should provide potentials appropriate to calculate at least the ^{209}Bi total neutron cross sections at higher energies and to examine the energy dependence of J_v.

Mahaux and Sartor[42] have recently studied the volume-integral-per-nucleon of the real potential for ^{208}Pb over the energy range 4.0–40.0 MeV by fitting a quadratic function of the energy to 23 experimental values. Since here the interest is in a potential valid for $E\gtrsim 10.0$ MeV, the calculation was repeated using the 15 values they considered appropriate in the 9.0–40.0 MeV region. From this calculation one finds

$$J_v=(402.6-2.35\times E-0.0105\times E^2)\ \text{MeV fm}^3\ . \tag{15}$$

At 10.0 MeV $dJ_v/dE=-2.56$ fm^3—a value quite similar to the $-2.2(\pm0.36)$ fm^3 found by Rapaport[29] in his global analysis of 7.0–30.0 MeV neutron data. On the other hand, the Mahaux and Sartor analysis,[42] which

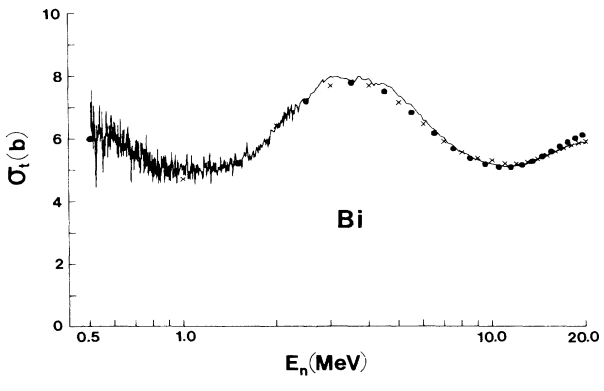

FIG. 8. Comparisons of measured and calculated neutron total cross sections of bismuth. The solid curve indicates the experimentally based evaluation of Ref. 43. The $\times$'s are the results calculated from the conventional model using Eqs. (4), (5), (9), and (12) below 10.0 MeV and the high-energy description given by Eqs. (4), (16), and (18) above 10.0 MeV. The solid data symbols represent results calculated with the model of Sec. IV B described by Eqs. (4), (8), (10), (23), and (24).

added only eight additional J_v values in the 4.0–7.0 MeV range, gives a much larger slope at 10.0 MeV ($dJ_v/dE = -3.67$ fm^3). The fact that the addition of these eight values can change the slope by such a large amount indicates that dJ_v/dE for the low-energy ^{208}PB data is much larger in magnitude than that needed to fit the high-energy results. The present ^{209}Bi analysis supports this finding since it also leads to a rather large value of dJ_v/dE below 10.0 MeV, e.g., as indicated by Eq. (12).

Thus, to predict the ^{209}Bi total cross sections at energies $\gtrsim 10.0$ MeV it is appropriate to deduce the parameters of the requisite optical model from the same data that led to Eq. (15). Assuming at most a quadratic energy dependence, a least-squares fit to the data yields

$$\begin{aligned} V_v &= (44.634 + 0.106\times E - 4.763\times 10^{-3}\times E^2)\ \text{MeV}\ , \\ r_v &= (1.2311 - 8.039\times 10^{-4}\times E - 3.670\times 10^{-5}\times E^2)\ \text{fm}\ , \end{aligned} \tag{16}$$

$$\begin{aligned} a_v &= (0.7658 - 6.864\times 10^{-3}\times E + 1.634\times 10^{-4}\times E^2)\ \text{fm}\ , \\ J_w &= (39.985 + 1.498\times E - 6.337\times 10^{-2}\times E^2)\ \text{MeV fm}^3\ , \end{aligned} \tag{17}$$

$$\begin{aligned} W_0 &= (5.780 + 0.109\times E - 6.430\times 10^{-3}\times E^2)\ \text{MeV}\ , \\ r_w &= (1.470 - 2.569\times 10^{-2}\times E + 6.627\times 10^{-4}\times E^2)\ \text{fm}\ , \\ a_w &= (0.4442 + 1.704\times 10^{-2} \\ &\quad \times E - 3.498\times 10^{-4}\times E^2)\ \text{fm}\ , \end{aligned} \tag{18}$$

where E is the incident energy in MeV. The geometric parameters of this optical potential intersect those of our 1.5–10.0 MeV analysis, Eq. (5), at $E = 7.86$, 7.78, 8.89, and 9.55 MeV for r_v, r_w, a_v, and a_w, respectively. Furthermore, the value of J_v obtained from Eq. (15) becomes equal to that given by Eq. (12) in this same energy region (i.e., $E = 8.10$ MeV). It is only the imaginary strengths, J_w, that intersect outside the 8.0–10.0 MeV energy range, and then not by much [Eqs. (9) and (17) become equal at 13.0 MeV]. It appears that a transition between the present low-energy potential and the high-energy ^{208}Pb one takes place in the 8.0–10.0 MeV energy range. Clearly a change in slope of the J_v versus E curve is indicated.

If one uses the potentials of Eqs. (16) and (18), together with the spin-orbit interaction of Eq. (4), a rather inferior description of the present 8.03 MeV experimental results is obtained. However, at 10.0 MeV a result quite comparable with that shown in Fig. 3 is obtained. Furthermore, the optical model described by these equations leads to predicted ^{209}Bi total cross sections in the 10.0–20.0 MeV range that are always within 2% of the experimental values,[43,44] as indicated by the ×'s in Fig. 8. Thus an excellent fit to the total cross section data can be obtained from a few hundred keV to 10 MeV using the potential described by Eqs. (4), (5), (9), and (12). The largest differences between measured and calculated values occur near 3.0 MeV where there appears to be some residual fluctuation in the experimental values. In addition, the observed elastic-scattering angular distributions are very well represented, as shown in Fig. 3. Making the transition to the higher-energy model of Eqs. (16) and (18), one extends the good representation of the total cross section to 20.0 MeV. Further extrapolation to higher energies is doubtful because Eq. (18) contains no volume absorption.

B. Surface-peaked real potential

Figure 9 shows the total volume-integral-per-nucleon of the real potential, J_v, which is the sum of the Woods-Saxon part, J_{WS}, and the surface component, $\lambda(E)J_w$, where $\lambda(E)$, J_w, and J_{WS} are shown in Fig. 5. Assuming a linear energy dependence, a best fit to the 4.5–10.0 MeV data gives

$$J_v = [(442.50\pm 2.57) - (7.27\pm 0.34)\times E]\ \text{MeV fm}^3\ . \tag{19}$$

Again, the data for $E \gtrsim 3.0$ MeV are well represented by this straight line, but below ≈ 3.0 MeV the J_v values lie consistently below the predictions of Eq. (19). In the conventional model the deviation of the lowest-energy points from the straight line given by Eq. (6) was $<2\%$, while in this case the discrepancy is somewhat larger ($<3\%$). If a linear fit is made to all of the data one finds

$$J_v = [(432.27\pm 1.18) - (5.89\pm 0.23)\times E]\ \text{MeV fm}^3\ . \tag{20}$$

Even with this fit, indicated by the b line in Fig. 9, the experimentally derived values lie below the curve for $E \lesssim 2.5$ MeV, but now the discrepancy is at the 1% level. Thus, again, it is hard to support a definitive deviation from linearity of J_v from a study of the 1.5–10.0 MeV neutron-scattering data.

The values of J_v needed to give the correct binding energies[36,37] for the seven known single-particle states and the six hole states in ^{208}Pb are shown in Fig. 9. In carrying out these calculations it was assumed that the geometry of the surfaced-peak real potential is given by the $E = 0$ limit of Eq. (10). The values of $\lambda(E)$ and J_w were computed, for these negative energies, from the principal-value integral of Eq. (8) and with the assumption that J_w is a quadratic function of $(E - E_F)$ near the Fermi surface, E_F, i.e.,

$$J_w = [0.969(E + 5.65)^2]\ \text{MeV fm}^3\ . \tag{21}$$

With this part of the potential fixed, the Woods-Saxon depth was varied so as to reproduce the observed binding energies when $a_v = 0.68$ fm and $r_v = 1.28$ fm, the values given by Eq. (10) when $E = 0$. The resulting J_v values, shown by ○'s in Fig. 9, clearly fall below the linear extrapolations of either Eq. (19) or (20). Indeed, the average value of J_v for the single-particles states, $J_v = 425.7$ MeV fm^3 with an rms deviation of ± 6.7 MeV fm^3, is only slightly larger than the value found at the lowest neutron energies, $J_v \cong 420$ MeV fm^3.

Curve c in Fig. 9 shows a semitheoretical estimate of J_v,

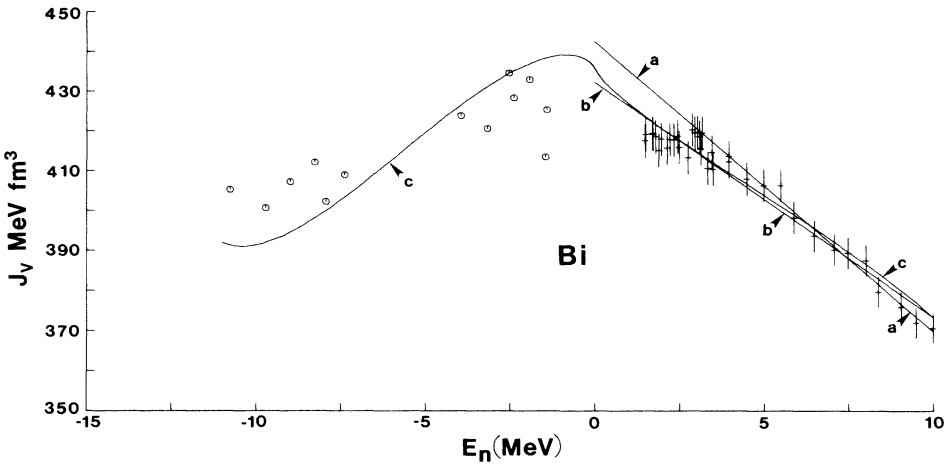

FIG. 9. The values of the total volume-integral-per-nucleon, J_v (in MeV fm^3), of the real potential discussed in Secs. IV B and V B of the text. The values at positive energies, + symbols, were obtained by fitting the ^{209}Bi elastic-scattering data. Curve *a* is a fit to these results over the 4.5–10.0 MeV energy range, Eq. (19), while curve *b* is a fit to all neutron-scattering data, Eq. (20). The negative-energy values were obtained from a fit to the observed binding energies of particle and hole states. The states considered, in order of increasing binding energy, were $2d_{3/2}$, $1g_{7/2}$, $3s_{1/2}$, $2d_{5/2}$, $0j_{15/2}$, $0i_{11/2}$, $1g_{9/2}$, $2p_{1/2}$, $1f_{5/2}$, $2p_{3/2}$, $0i_{13/2}$, $1f_{7/2}$, and $0h_{9/2}$. The values shown by ○'s were obtained using a Woods-Saxon potential with $a_v=0.68$ fm and $r_v=1.28$ fm. Curve *c* is the prediction of Eq. (22) when J_{WS} has the energy dependence of Eq. (23) for $E>0$ and is a constant, $J_{WS}=415.08$ MeV fm^3, for all negative energies.

$$J_v = J_{WS} + \lambda(E) J_w \ , \tag{22}$$

obtained when $\lambda(E)$ is given by the principal-value integral of Eq. (8), and J_w is given by Eq. (9) for $E \geq 0$, and by Eq. (21) for $-11.0 \leq E \leq 0$ MeV. For $E \geq 0$, J_{WS} in Eq. (22) was taken to be

$$J_{WS} = (415.08 - 3.81 \times E) \text{ MeV fm}^3 \ , \tag{23}$$

which is the best fit to all the neutron-scattering data. However, for $E<0$ it was assumed to have the constant value, 415.08 MeV fm^3. For $E \gtrsim 1.5$ MeV the predicted values of J_v are almost identical to those given by either Eq. (19) or (20), and for $E<0$ the curve comes quite close to the J_v values needed to give the correct binding energies. Thus over the energy range -11.0 to $+10.0$ MeV the energy dependence of J_v predicted by Eq. (22) is quite close to that needed to fit the experimental values and, furthermore, the point at which $dJ_v/dE=0$ is predicted to occur at negative energy. [If the energy-dependent geometry of the Woods-Saxon well given by Eq. (10) had been used, somewhat larger values of J_v would have been obtained but still smaller than those given by extrapolating either Eq. (19) or (20) to negative energies. For this case the J_v values predicted by Eq. (22) follow closely those needed to reproduce the observed binding energies provided J_{WS}, given by Eq. (23), is used for all energies. In this calculation the point at which $dJ_v/dE=0$ again occurs at negative energy.]

When the model described by Eqs. (4), (8), (10), and (11) is used, the calculated *S*-wave strength function is a factor of 2 larger than deduced from resonance measurements. On the other hand, a reasonable description of the neutron total cross section is achieved down to at least 500 keV. A result somewhat closer to experiment can be obtained if one uses J_{WS} given by Eq. (23), together with the best fit to all the J_w values shown in Fig. 5(b),

$$J_w = [(29.53 \pm 0.97) + (1.58 \pm 0.23) \times E] \text{ MeV fm}^3 \ . \tag{24}$$

When these strengths are used, in conjunction with the geometry of Eq. (10), the predicted total cross section is shown by the ●'s in Fig. 8.

In order to evaluate the strength of the surface real potential, $\lambda(E)$ of Eq. (8), it was necessary to know the form of $W(r,E)$ at all energies. Since first-hand knowledge of $W(r,E)$ extended only to 10 MeV, it was assumed that for $E>10.0$ MeV the surface imaginary potential of Walter and Guss[27] was appropriate. Thus, inherent in the present model is the assumption that above 10.0 MeV neither the imaginary strength given by Eq. (11) nor (24) is appropriate, but instead the parameters of the surface-imaginary potential are

$$\begin{aligned} W_0 &= (7.776 - 0.157 \times E) \text{ MeV} \ , \\ r_w &= 1.282 \text{ fm} \ , \\ a_w &= 0.512 \text{ fm} \ , \end{aligned} \tag{25}$$

as given in Ref. 27. Extrapolation of the present model above 10.0 MeV implies that one should use the surface absorption of Eq. (25), the value of $\lambda(E)$ calculated from Eq. (8), and a real Woods-Saxon well with the geometry of Eq. (10) and strength given by Eq. (23). When this is combined with the volume absorption of the Walter and Guss potential, the result is a poor fit to the total-cross-section data above ≈ 10.0 MeV. On the other hand, if

one does not worry about self consistency and instead calculates the value of $\lambda(E)$, assuming the Walter and Guss interaction, and then uses that value in conjunction with the geometry and strength of the imaginary potential given by Eqs. (10) and (24), a good description (within $\approx 2\%$) of the total cross section is obtained up to 17.5 MeV. Furthermore, a suitable description of the 11.2 MeV elastic-scattering data of Ferrer *et al.*[45] is obtained except at four angles ($\approx 110°$, 115°, 150°, and 155°) out of thirty, and even in these instances the differences between calculations and experiment are only a few mb/sr.

When the conventional optical model is used to interpret the data, it is possible to show that the description of the high-energy ^{208}Pb experiments, when combined with the lower-energy ^{208}Pb and ^{209}Bi data, implies a change in dJ_v/dE in the neighborhood of 10.0 MeV. Although several analyses of high-energy ^{208}Pb data have been made[9,38] using the real surface-peaked potential model, they cannot be easily connected with the present treatment of the ^{209}Bi data because of the differences in the way $\lambda(E)$, Eq. (8), was calculated. As suggested by Mahaux and Ngô,[3] J_w in the present analysis was assumed to be symmetric about the Fermi energy, E_F, and as a consequence a significant negative contribution to the dispersion integral is obtained from values of $E' < 0$. This causes $\lambda(E)$ to change sign at approximately 9.0 MeV in the present model. However, in the work of Annand *et al.*[9] only the contribution to the principal-value integral for $E' > 0$ was included. Implicitly they assumed that $W(r,E')$ dropped discontinuously to zero for $E' \leq 0$, which not only leads to a discontinuity in $\lambda(E)$ at $E = 0$ but also has the consequence that $\lambda(E)$ does not get the large negative contribution from the principal-value integral. Therefore, their $\lambda(E)$ goes through zero at a much higher energy than that of the present work (≈ 20 MeV). In the analysis of Finlay *et al.*,[38] the strength of the surface real potential was taken to be 0.24 times the values calculated by Ahmad and Haider.[46] These latter authors used the surface absorption potential appropriate for proton scattering from ^{40}Ca, and assumed $W(r,E')$ went to zero at $E' = 0$. $\lambda(E)$ calculated in this way changes sign at approximately 30.0 MeV. Moreover, the data for ^{40}Ca cannot be used in a self-consistent description of ^{208}Pb. Thus, until one has calculations for both low-energy ^{209}Bi and high-energy ^{208}Pb data that use the same ground rules for evaluating $\lambda(E)$, it is not possible to demonstrate a change in the magnitude of dJ_v/dE in the 10.0 MeV region from an analysis of the neutron-scattering data using the surface-peaked real-potential model.

VI. SUMMARY

The neutron differential elastic-scattering cross sections of ^{209}Bi were measured from 4.5 to 10.0 MeV at incident neutron energy intervals of ≈ 0.5 MeV and at 40 or more scattering angles distributed between $\approx 18°$ and 160°. Particular attention was given to the specification of the uncertainties necessary for rigorous fitting of the data to obtain model parameters. The present experimental results were combined with the lower-energy distributions previously reported from this laboratory,[5] and with those reported by Olsson *et al.*,[6] to obtain a comprehensive experimental elastic-scattering data base extending from ≈ 1.5 to 10.0 MeV. This data base was interpreted in terms of the spherical optical-statistical model with and without the surface-peaked component of the real potential required by the dispersion relation.[2] The main conclusions reached from these analyses were:

(i) Properties of the real optical-model potential. In order to fit the ^{209}Bi data over the 1.5–10.0 MeV energy range, the radius of the Woods-Saxon well, r_v, used for the volume part of the potential must decrease with increasing energy. In the case of the conventional analysis, this decrease is quite strong [see Eq. (5)]. When the surface-peaked real potential is added, the decrease in r_v with increasing energy remains, but is much less rapid as can be seen from a comparison of Eqs. (5) and (10). For both models the diffuseness of the real well could have been taken to be energy independent, although with the conventional model a slightly better fit to the data was obtained with the energy dependence given by Eq. (5). The volume integral of the Woods-Saxon potential, J_{WS}, of the surface-peaked model decreases in value as the energy, E, increases, with $dJ_{WS}/dE = -3.81$ fm^3 when a best fit to all the data is made. This appreciable slope is to be contrasted with $dJ_{WS}/dE \approx 0$ found in the analysis of the yttrium data.[25] The total volume-integral-per-nucleon of the real potential, J_v, decreases with increasing energy, the slope depending upon the model used in the analysis of the data [compare Eqs. (12) and (20)]. Over the energy range 3.0–10.0 MeV, for either model, this slope was constant. Below 3.0 MeV, dJ_v/dE seems to decrease in magnitude, as shown in Figs. 4 and 9, but it remains negative to at least 1.5 MeV.

(ii) Properties of the imaginary optical-model potential. Below 10 MeV the imaginary interaction was described by a Woods-Saxon-derivative well. No evidence for volume absorption was found. The behavior of the imaginary interaction was similar for both the conventional and surface-peaked models. The potential radius was energy independent, whereas the diffuseness varied rapidly with energy as can be seen from Eqs. (5) and (10). Near zero energy the imaginary potential approaches a delta function, while in the 8.0–10.0 MeV region it displays a diffuseness characteristic of that found in a global analysis of neutron-scattering data.[29] J_w, the volume-integral-per-nucleon of the imaginary potential, is small, as is characteristic of nuclei near closed shells,[31] and it increases slightly with increasing energy. Below 3.0 MeV, the J_w values, illustrated in Figs. 4 and 5(b), exhibit some scatter which may be due to residual compound-nucleus fluctuations.

(iii) Fermi surface anomaly. According to Mahaux and Ngô,[3] the total volume-integral-per-nucleon of the real potential, J_v, should have a slope $dJ_v/dE = 0$ at approximately 4.0 MeV incident-neutron energy. Our analyses of the ^{209}Bi data show that between 3.0 and 10.0 MeV dJ_v/dE is constant and has a value between -6.0 and -9.0 fm^3, depending upon which model is used to

analyze the data. Below 3.0 MeV, dJ_v/dE seems to decrease in magnitude, and this is consistent with the values of J_v needed to give the correct binding energies of single-particle and single-hole states, as shown in Fig. 9. Annand *et al.*[9] analyzed some of the same low-energy neutron-scattering data used in the present interpretation (that of Ref. 6) and reported a change in sign of dJ_v/dE at positive energies below 3.0 MeV. The present analysis of the same data, resulting in better fits to the measured values, indicated a reduction of dJ_v/dE below 3.0 MeV but no change of sign. Thus only when the low-energy neutron-scattering data are considered in conjunction with the bound-state energies does one have clear evidence of the Fermi surface anomaly.

(iv) J_v versus E curve near 10.0 MeV. As noted above, the present analysis of the ^{209}Bi data below 10.0 MeV results in large values of dJ_v/dE, -6.0 to -9.0 fm^3. On the other hand, a fit to all the ^{208}Pb data above 9.0 MeV, similar to that carried out by Mahaux and Sartor,[42] leads to $dJ_v/dE \approx -2.6$ fm^3 at $E \approx 10.0$ MeV. This latter value is quite close to the global value, $dJ_v/dE = -2.28$ fm^3, reported by Rapaport[29] from an analysis of 7.0–30.0 MeV neutron-scattering data. By combining the ≤ 10.0 MeV ^{209}Bi and ≥ 10.0 MeV ^{208}Pb results, it is clear that in the vicinity of 10 MeV dJ_v/dE makes a transition from a relatively large negative slope to a smaller negative value characteristic of higher-energy interpretations. Furthermore, the geometrical parameters of the low-energy ^{209}Bi potential become equal to those of the high-energy ^{208}Pb interaction in the same energy range. If one carefully examines the calculational results of Mahaux and Ngô,[3] one sees that they predict a change of this nature in the region of 15.0 MeV incident-neutron energy. The combination of the analyses of the ^{208}Pb and ^{209}Bi data, together with the interpretation of bound-state potentials, leads to an energy dependence of J_v quite similar to that predicted by Mahaux and Ngô, but shifted downward in energy by about 5.0 MeV.

(v) Low-energy/high-energy dichotomy. From an analysis of S-wave strength functions and neutron scattering and polarization data at low energies, Moldauer[47] concluded that the absorptive part of optical-model potential was sharply peaked near the nuclear surface (i.e., a_w was small) and r_v was greater than 1.26 fm for all but the transuranic elements. These results are in marked contrast to the global values,[29] $r_v = 1.198$ fm and $a_w = 0.59$ fm, arising from a fit to the 7–30 MeV neutron-scattering data. The present ^{209}Bi and ^{208}Pb analysis provides another example of this dichotomy. If the low-energy variation of these parameters with energy is rapid whereas the high-energy variation is slight, as found in the present analysis, this has important ramifications with respect to the extrapolation between low- and high-energy optical-model parameters.

ACKNOWLEDGMENTS

The authors are indebted to Mr. J. Fabish, Mr. J. Whalen, and Mr. A. Engfer for their assistance and consultation in the above work. A detailed work of this work is given in Argonne National Laboratory Report ANL/NDM-100 (1987). This work was supported by the U.S. Department of Energy under Contract W-31-109-Eng-38.

[1] J. Blomqvist and S. Wahlborn, Ark. Fys. **16**, 545 (1960).
[2] See, for example, G. R. Satchler, *Direct Nuclear Reactions* (Clarendon, Oxford, 1983).
[3] C. Mahaux and H. Ngô, Nucl. Phys. **A378**, 205 (1982); Phys. Lett. **100B**, 285 (1981).
[4] E. Barnard, J. deVilliers, D. Reitmann, A. Smith, and J. Whalen, Nucl. Sic. Eng. **41**, 63 (1970).
[5] P. Guenther, A. Smith, and J. Whalen, Nucl. Sci. Eng. **75**, 69 (1980).
[6] N. Olssson, B. Holmqvist, and E. Ramstrom, Nucl. Phys. **A385**, 285 (1983).
[7] C. Zafiratos, T. Oliphant, J. Levin, and L. Cranberg, Phys. Rev. Lett. **14**, 913 (1965).
[8] B. Holmqvist and T. Wiedling, Aktiebolaget Atomenergi Repot No. AE-430, 1971 (unpublished).
[9] J. Annand, R. Finlay, and F. Dietrich, Nucl. Phys. **A443**, 249 (1985).
[10] C. Budtz-Jørgensen, P. Guenther, A. Smith, J. Whalen, W. McMurray, M. Renan, and I. van Heerden, Z. Phys. **A319**, 47 (1984).
[11] A. Smith, P. Guenther, J. Whalen, I. van Heerden, and W. McMurray, J. Phys. G **11**, 125 (1985).
[12] A. Smith, P. Guenther, R. Larsen, C. Nelson, P. Walker, and J. Whalen, Nucl. Instrum. Methods **50**, 277 (1967).
[13] M. Drosg, in *Proceedings of the Advisory Group Meeting on Neutron Source Properties, Leningrad, 1986,* edited by K. Okamoto (IAEA, Vienna, 1986), p. 13.
[14] A. Smith, P. Guenther, and R. Sjoblum, Nucl. Instrum. Methods **140**, 397 (1977).
[15] IAEA Technical Report 227, 1983.
[16] P. T. Guenther, Ph.D. thesis, University of Illinois, 1977.
[17] A. Smith and P. Guenther, Argonne National Laboratory report (unpublished).
[18] R. M. Wilenzick, K. K. Seth, P. R. Bevington, and H. W. Lewis, Nucl. Phys. **62**, 511 (1965).
[19] J. R. Beyster, M. Walt, and E. W. Salmi, Phys. Rev. **104**, 1319 (1956).
[20] P. E. Hodgson, *Nuclear Reactions and Nuclear Structure* (Clarendon, Oxford, 1971).
[21] W. Hauser and H. Feshbach, Phys. Rev. **87**, 366 (1952).
[22] P. A. Moldauer, Nucl. Phys. **A344**, 185 (1980).
[23] *Table of Isotopes,* 7th ed., edited by C. M. Lederer and V. S. Shirley (Wiley, New York, 1978).
[24] A. Gilbert and A. Cameron, Can. J. Phys. **43**, 1446 (1965).
[25] R. D. Lawson, P. T. Gunether, and A. B. Smith, Phys. Rev. C **34**, 1599 (1986).
[26] R. Sartor and C. Mahaux, Phys. Rev. C **21**, 1546 (1980).
[27] R. L. Walter and P. P. Guss, in *Nuclear Data for Basic and Applied Science,* edited by P. G. Young, R. E. Brown, G. F. Auchampaugh, P. W. Lisowski, and L. Stewart (Gordon and Breach, New York, 1986), Vol. 2, p. 1079.
[28] G. Bulski, W. Grum, J. Hammer, H. Postner, G. Schleussner,

and E. Speller, in *Proceedings of the Antwerp Conference on Nuclear Data for Science and Technology,* Dordrecht, 1982, edited by K. H. Böckhoff (Reidel, Dordrecht, 1982), p. 783.
[29]J. Rapaport, Phys. Rep. **87**, 25 (1982).
[30]A. B. Smith, P. T. Guenther, and R. D. Lawson, Nucl. Phys. **A455**, 344 (1986).
[31]A. M. Lane, J. Lynn, E. Melkonian, and E. Rae, Phys. Rev. Lett. **2**, 424 (1959); W. Vonach, A. Smith, and P. Moldauer, Phys. Lett. **1**, 331 (1964); A. Smith, P. Guenther, and J. Whalen, Nucl. Phys. **A415**, 1 (1984).
[32]J. Tepel, H. Hofmann, and H. Weidenmuller, Phys. Lett. **49B**, 1 (1974).
[33]H. Hofmann, J. Richert, J. Tepel, and H. Weidenmuller, Ann. Phys. (N.Y.) **90**, 403 (1975).
[34]M. Zirnbauer, in *Proceedings of the Conference on Neutron-Nucleus Collisions, A Probe of Nuclear Structure,* New York, 1985, edited by J. Rapaport, R. Finlay, S. Grimes, and F. Dietrich, AIP Conf. Proc. No. 124 (AIP, New York, 1985), p. 481.
[35]S. Cierjacks, P. Forti, D. Kopsch, L. Kropp, J. Nebe, and H. Unseld, Kernforschung Karlsruhe Report KFK-1000, 1968 (unpublished).
[36]A. H. Wapstra and K. Bos, At. Data Nucl. Data Tables **19**, 177 (1977).
[37]M. R. Schmorak and R. L. Auble, Nucl. Data Sheets **B5**, 205 (1971).
[38]R. W. Finlay, J. R. M. Annand, T. S. Cheema, J. Rapaport, and F. S. Dietrich, Phys. Rev. C **30**, 796 (1984).
[39]C. Mahaux and R. Sartor, Phys. Rev. Lett. **57**, 3015 (1986).
[40]S. Mughabghab, M. Divadeenam, and N. E. Holden, *Neutron Cross Sections* (Academic, New York, 1981), Vol. 1, Pt. B.
[41]C. E. Porter, Phys. Rev. **100**, 935 (1955).
[42]C. Mahaux and R. Sartor, Phys. Rev. C **34**, 2119 (1986).
[43]O. Bersillon, B. Caput, and C. Philis, in *Proceedings of the Antwerp Conference on Nuclear Data for Science and Technology,* Dordrecht, 1982, edited by K. H. Böckhoff (Reidel, Dordrecht, Holland, 1982), p. 665.
[44]A. Smith, P. Guenther, D. Smith, J. Whalen, and R. Howerton, Argonne National Laboratory Report No. ANL/NDM-51, 1980 (unpublished).
[45]J. C. Ferrer, J. D. Carlson, and J. Rapaport, Nucl. Phys. **A275**, 325 (1977).
[46]I. Ahmad and W. Haider, J. Phys. G **2**, L157 (1976).
[47]P. A. Moldauer, Nucl. Phys. **47**, 65 (1963).